

Empowering Dynamic Urban Navigation with Stereo and Mid-Level Vision

Wentao Zhou, Xuweiyi Chen, Vignesh Rajagopal,
Jeffrey Chen, Rohan Chandra, Zezhou Cheng
University of Virginia

<https://www.cs.virginia.edu/~tsx4zn/stereowalk/>

Abstract

The success of foundation models in language and vision motivated research in fully end-to-end robot navigation foundation models (NFM). NFM directly map monocular visual input to control actions and ignore mid-level vision modules (tracking, depth estimation, etc) entirely. While the assumption that vision capabilities will emerge implicitly is compelling, it requires large amounts of pixel-to-action supervision that are difficult to obtain. The challenge is especially pronounced in dynamic and unstructured settings, where robust navigation requires precise geometric and dynamic understanding, while the depth-scale ambiguity in monocular views further limits accurate spatial reasoning. In this paper, we show that relying on monocular vision and ignoring mid-level vision priors is inefficient.

We present **StereoWalker**, which augments NFM with stereo inputs and explicit mid-level vision such as depth estimation and dense pixel tracking. Our intuition is straightforward: stereo inputs resolve the depth-scale ambiguity, and modern mid-level vision models provide reliable geometric and motion structure in dynamic scenes. We also curate a large stereo navigation dataset with automatic action annotation from Internet stereo videos to support training of StereoWalker and to facilitate future research. Through our experiments, we find that mid-level vision enables StereoWalker to achieve a comparable performance as the state-of-the-art using only 1.5% of the training data, and surpasses the state-of-the-art using the full data. We also observe that stereo vision yields higher navigation performance than monocular input.

1. Introduction

Embodied visual navigation (mapping pixels to velocity/acceleration) in urban environments is a popular area of research due to its capacity to enable direct, end-to-end deployment, which is useful for real-world applications such as last mile delivery. Despite rapid progress, visual naviga-

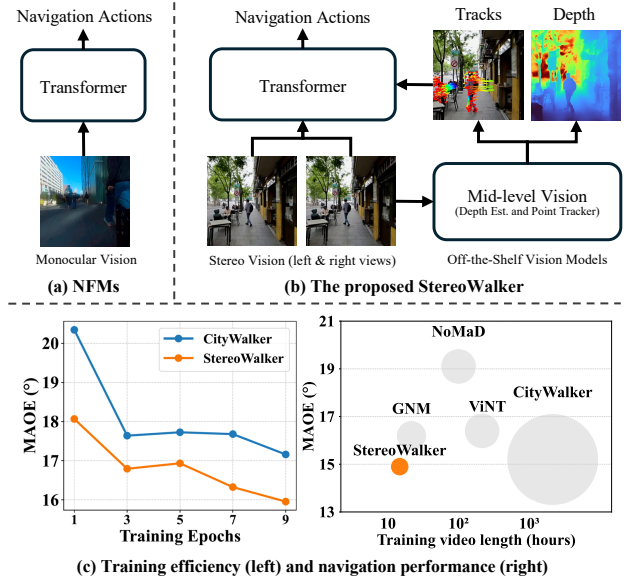


Figure 1. **Overview.** (a) Existing visual navigation foundation models (NFM) process monocular inputs and predict actions without any intermediate vision modules. (b) StereoWalker improves this paradigm by incorporating stereo and mid-level vision modules such as depth estimation and dense point tracking. (c) Relative to CityWalker, the current state of the art, StereoWalker reaches high training efficiency and improved navigation accuracy while using only 1.5% of the training data.

tion performs poorly in dynamic and unstructured environments, which involve dense and diverse pedestrian movements, irregular roadside configurations, and an open-world variety of object categories. Navigating dynamic unstructured environments effectively requires a comprehensive and accurate understanding of 3D scene semantics, geometry, and dynamics, adherence to common-sense rules and social conventions, such as using sidewalks, obeying traffic signals, and keeping appropriate interpersonal distance.

Early visual navigation approaches [20, 34, 44, 47] build on modular vision systems for detection, tracking, and planning, yet their performance was constrained by hard-coding

rule-based decision making and evaluations confined to simple or near-static environments. Reinforcement learning in photorealistic simulators [4, 24, 31, 55, 67–70] achieved progress but still suffers from the sim-to-real gap. Recent efforts [57, 58, 62] introduced visual navigation foundation models (NFMs) that learn from expert demonstrations to map visual inputs directly to actions, however, their scalability remains constrained by the scarcity of pixel-to-action supervision. More recently, CityWalker [39] addressed this limitation by automatically mining and annotating human navigation videos from the Internet. Although NFMs trained on such in-the-wild data achieved impressive improvements, their robustness in dynamic and unstructured environments remains poor for two reasons: (1) NFMs use monocular input which introduces depth-scale ambiguity resulting in annotation noise and performance bottlenecks. For real-world robot navigation, accurate depth is critical for safety [10, 16], which is why most robotic platforms typically include stereo cameras and (2) NFMs assume that mid-level vision priors, which are necessary for providing structure to the predicted outputs, would emerge implicitly. However, this is a strong assumption and prior work in other robotic domains [9, 45, 46, 56, 73, 76, 80] has concluded that explicit mid-level supervision improves performance.

Therefore in this work, we propose to empower NFMs with stereo and mid-level vision. Our work is guided by two key insights: First, **stereo inputs resolve the depth-scale ambiguity inherent in monocular perception**. Adding stereo input improves navigation success and reduces error in a number of critical navigation scenarios. **Second, mid-level vision improves generalization, stability, and data efficiency**. StereoWalker surpasses the state-of-the-art, CityWalker [39], *using only 1.5% of its training data* (Fig. 1), highlighting the impact of stereo and mid-level vision on scalable and robust urban navigation.

Main Contributions: In summary,

- We present StereoWalker, a visual NFM built on stereo inputs and structured with explicit mid-level vision modules, achieving state-of-the-art performance in overall navigation.
- We release a new stereo dataset of pedestrians walking in global metropolitan cities. We additionally develop a filter using vision-language models removing contents that do not contain goal-directed walking.
- We demonstrate our approach on established benchmark (CityWalker), our new benchmark (StereoWalker), and in real world environments.

2. Related Work

Embodied Navigation Tasks. Embodied navigation tasks are commonly categorized by how the goal is specified. Existing paradigms include point-goal or position-goal navigation [6, 8, 19, 21, 25, 55, 66], image-

goal navigation [22, 33, 35, 43, 51, 54, 82], object-goal navigation [1, 5, 7, 18, 42], and vision-language navigation [15, 32, 49, 63, 78, 79]. Our work follows the position-goal formulation, where navigation is defined through ordered waypoints in Euclidean space. While in public urban spaces, recent foundation models for visual navigation [39, 57, 58, 62] have shown encouraging performance across these paradigms, they often abstract away the fine-grained visual structure of the scene, relying on compressed global features or language-conditioned embeddings. In contrast, the embodied navigation task inherently depends on rich visual understanding (*e.g.*, geometry, motion, and spatial layout), all of which are observable in the image stream but only partially exploited in most current approaches. The focus of our formulation is therefore on examining how a model can more completely utilize visual information to infer spatial transitions between successive waypoints.

Mid-level Vision for Robotics. Prior studies [9, 45, 46, 56, 73–76, 80] have shown that mid-level visual representations can improve generalization and data efficiency across a wide range of robotic tasks. Early works [9, 45, 46, 73, 76] demonstrated that supplying sensorimotor policies with geometric and semantic cues such as optical flow, depth, and segmentation leads to better action prediction. Subsequent efforts [80] expanded this idea to diverse tasks in simulation, showing that mid-level features often outperform raw pixels and reduce sample complexity. Other approaches [9] explored their use in manipulation, grasping, and navigation, highlighting their value relative to strategies like domain randomization. However, most of these studies were conducted in simplified or static environments and preceded the emergence of navigation foundation models. Our work revisits this line of inquiry in the context of real-world dynamic urban navigation and provides evidence that explicit mid-level vision remains essential for scalable and reliable end-to-end navigation models.

Stereo Vision for Robotics. Modern navigation systems incorporate diverse sensing modalities such as LiDAR for accurate three dimensional geometry [52, 71, 81], event cameras for high frequency motion cues [17, 23], and multi camera setups for broad spatial coverage [26, 38]. Stereo cameras offer a practical alternative, providing accurate depth with passive sensing, low cost, and simple deployment, which has led to their broad use in robotics [30, 60]. Stereo perception supports a range of robot learning tasks, including manipulation and grasping [2, 13, 29, 59], industrial assembly and insertion [3, 11, 41, 61], and dynamic locomotion and whole body control [14, 37, 77]. Our work leverages stereo video as large scale training data for navigation, using geometric cues as implicit visual context rather than direct sensory measurements.

3. Stereo Urban Navigation Dataset

While stereo sensing is widely used in robotic perception, it remains underexplored in embodied urban navigation, where most visual models rely on monocular or depth-simulated imagery. To bridge this gap, we curate a large-scale training dataset from stereoscopic walking videos mined from publicly available YouTube content under the Standard License. We focus on high-resolution VR180 first-person videos, which naturally provide egocentric stereo geometry suitable for learning visuomotor representations.

Our dataset includes roughly 500 independent and non-overlapping clips, totaling 60 hours of stereo footage spanning multiple global cities such as San Francisco, Madrid, and Tokyo. Compared to the monocular data in CityWalker [39], which was captured within a single metropolitan region, our collection offers broader diversity in architectural layouts, lighting, weather, and pedestrian density. Each video is filtered and rectified into left-right image pairs (I_i^L, I_i^R) indexed by frame $i \in [1, N]$, to ensure reliable geometric correspondence. Following practices in web-mined video datasets such as Stereo4D [27], we will release annotations, metadata, and video links under a CC license.

Filtering and Quality Control. We apply an automatic filtering stage to ensure that the collected videos capture goal-directed walking rather than passive observation or unrelated activities. Online walking footage often includes segments where the camera wearer pauses, interacts with bystanders, or engages in activities such as shopping or sightseeing.

CityWalker videos contain similar non-navigational content, which can introduce undesirable biases into learned navigation behaviors (see supplementary material). To remove these segments, we use a vision-language filtering model, Qwen2-VL [65], which analyzes visual content together with temporal context. For each candidate clip, the model reviews frames sampled at one frame per second, along with associated captions, and assesses whether the motion reflects forward locomotion toward an implicit goal. Only clips that consistently display egocentric, target-oriented walking are retained. The full filtering prompt is provided in the supplementary material.

The resulting dataset consists mainly of continuous walking sequences with clear ego-motion and minimal idle behavior. These filtered clips serve as the input to the subsequent trajectory estimation stage based on stereo visual odometry. We include precision and recall metrics to demonstrate the efficiency of our filtering approach in the supplementary material.

Action Labels from Videos. To derive action supervision for training our navigation foundation model, we compute

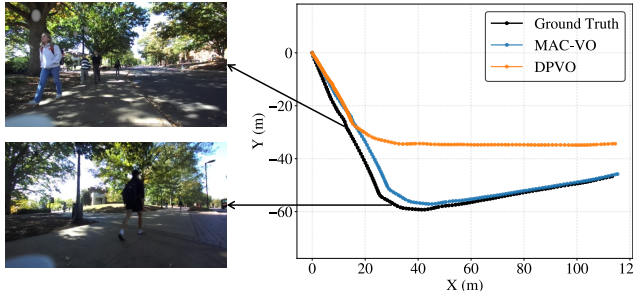


Figure 2. **Ground-truth Trajectory comparison: MAC-VO vs. DPVO.** We overlay the trajectories estimated by MAC-VO and DPVO; MAC-VO tracks the GT more closely with reduced drift and scale error, while DPVO shows larger deviations.

trajectory labels directly from the collected stereo videos using state-of-the-art stereo visual odometry (VO) methods. In particular, we adopt MAC-VO [50], which utilizes stereo input and surpasses other VO methods and SLAM in challenging scenarios. The resulting trajectories give higher quality camera translation compare to DPVO [64] which is used by CityWalker, as illustrated in Figure 2. This VO-based labeling pipeline can process large quantities of raw stereo footage without manual annotation or language-based prompting, enabling efficient expansion to large scale training data.

4. StereoWalker

Our model fuses mid-level vision foundation models and utilizes stereo information. In this section, we first discuss the task setting (Sec. 4.1); we then provide the details of StereoWalker (Sec. 4.2).

4.1. Preliminaries: Dynamic Urban Navigation

We study visual navigation in dynamic urban settings, where the objective is to generate a series of waypoints from the current location to a specified target. Urban environments introduce substantial challenges due to their complex visual structure and human and vehicle motion, which demands an understanding of geometry and dynamics from raw visual input. Following the task setup of previous urban navigation foundation models [39, 57, 58, 62], each training instance consists of a temporally ordered sequence of observations $\{V_i\}_{i=1}^N$, corresponding positions $\{\mathcal{P}_i \in \mathbb{R}^2\}_{i=1}^N$ and a sub-goal waypoint $\mathcal{P}' \in \mathbb{R}^2$. The learning objective is to approximate the following neural function:

$$F_\theta : (\mathcal{V}_{t-N+1:t}, \mathcal{P}_{t-N+1:t}, \mathcal{P}') \mapsto \mathcal{P}_{t+1:t+N},$$

where N denotes the length of a short temporal window of recent stereo observations and positions. Our model takes the current subgoal \mathcal{P}' as the immediate target and predicts the short-horizon trajectory that advances toward it. Once the model reaches \mathcal{P}' , the next waypoint in the predefined sequence becomes the new sub-goal, forming a continuous

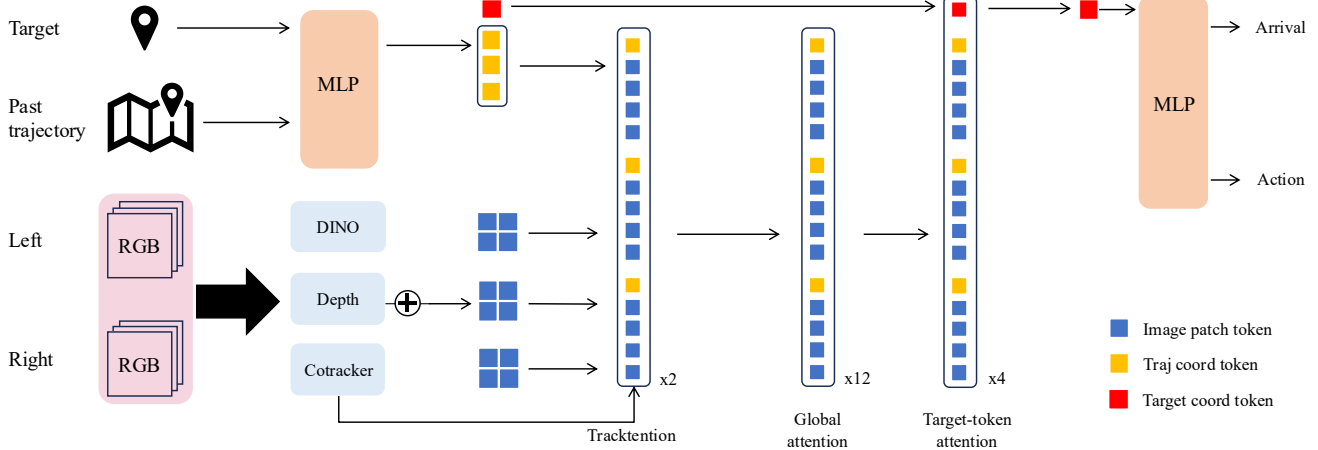


Figure 3. **Overview of StereoWalker’s Architecture.** StereoWalker takes in stereo image pairs with corresponding trajectory and a target position. The images first go through three vision foundation modules, where depth embeddings and DINO features are concatenated to get patch tokens. We then append position tokens and use trackings for Tracktention [36]. A global attention module further processes the tokens, followed by the target-token attention which merges all the information into the target token. Finally, an MLP converts the updated target token to arrival probability and action predictions.

waypoint-to-waypoint navigation process. This formulation can naturally scale to long-range navigation by chaining multiple waypoints obtained from a global path planner such as A^* and other graph-search based algorithms.

4.2. Model Design

Overview. While prior visual navigation models compress each frame to a single DINOv2 [CLS] token [48], StereoWalker retains *all* patch tokens to preserve fine-grained spatial structure critical for control. Our intuition is straightforward: accurate navigation demands richer visual perception than a global summary can provide.

As shown in Fig. 3, given a short temporal window of rectified stereo (or monocular) frames $\mathcal{V}_{t-N+1:t}$ and their corresponding positions $\mathcal{P}_{t-N+1:t}$, the model forms dense mid-level tokens that jointly encode appearance, geometry, and short-term motion cues. Tokens from all frames are then processed by three stages: (i) tracking-guided attention to maintain temporal correspondence and reduce drift, (ii) global attention to integrate scene context across views, and (iii) target-token attention to focus prediction on goal-relevant regions. StereoWalker supports both stereo and monocular inputs with the same architecture, differing only in tokenization.

Image tokenization. We employ three off-the-shelf foundation vision models to obtain complementary information from each frame in $\mathcal{V}_{t-N+1:t}$. Specifically, DINOv2 [48] provides high-level patch representations, DepthAnythingV2 [72] estimates per-pixel depth and CoTracker-v3 [28] generates point trajectories across time, where M_{trk} is the number of tracks. All the pretrained models are frozen in our architecture.

Depth aggregation. We design our depth module to be compatible for both monocular and stereo input. While DINOv2 computes hierarchical visual features, DepthAnythingV2 leverages these features to predict a per-pixel depth map Z_i . For stereo image pairs $(\mathcal{V}_i^L, \mathcal{V}_i^R)$, DepthAnythingV2 is also applied to the left image \mathcal{V}_i^L for the depth map, which is used to get a refined disparity map between the left and right views with a pretrained stereo matching network of MonSter++ [12]. The geometric relationship between disparity d and depth Z is given by $Z = \frac{fB}{d}$, where f denotes the focal length and B is the stereo baseline. The resulting disparity map is converted to a depth map, which is then patchified by a depth encoder into depth embeddings $\mathbf{z}_{j,k}$, with j and k indexing the spatial location of each patch in the image. We treat depth as an independent feature dimension rather than as a derivative of RGB texture. Accordingly, each image token is \mathbf{f} by concatenating the DINO-derived appearance embedding $\mathbf{x}_{j,k}$ and the depth embedding, producing $\mathbf{h}_{j,k} = [\mathbf{x}_{j,k}; \mathbf{z}_{j,k}]$ that jointly encodes photometric and geometric information.

Tracking-guided attention. To capture temporal correspondence across frames, we introduce a *tracking-guided attention* module inspired by TrackTention [36]. Given image tokens $\mathbf{H}_i = \{\mathbf{h}_{j,k}\}$ for each frame i within a temporal window $[t-N+1, t]$ and a set of point tracks $\mathbf{T}_i^{\text{trk}} = \{\mathbf{p}_{i,m}\}$ obtained from CoTracker-v3, where m denotes the number of tracks. This module integrates spatial appearance and temporal motion through three successive operations.

1) *Track-aware sampling.* Each 2D point $\mathbf{p}_{i,m}$ is embedded into a track token $\mathbf{q}_{i,m}^{\text{trk}}$ through positional encoding and projection. Using cross-attention between the track tokens and image tokens, the model aggregates local visual

evidence from \mathbf{H}_i into a set of sampled track features \mathbf{S}_i . This operation allows each track to selectively pool information from nearby spatial regions based on learned attention weights rather than fixed interpolation.

2) *Temporal propagation.* The track features $\mathbf{S}_{1:T}$ from consecutive frames are organized into sequences of length T for each track and processed by a transformer that performs self-attention along the temporal axis. The resulting representations $\tilde{\mathbf{S}}_{i,m}$ capture smooth temporal evolution of appearance and motion, reinforcing correspondence across occlusion or viewpoint changes.

3) *Feature update.* To update image features, we perform a second cross-attention where spatial coordinate embeddings $\mathbf{c}_{j,k}$ act as queries and the updated track tokens $\tilde{\mathbf{S}}_i$ serve as keys and values. This produces motion-aware corrections $\Delta\mathbf{H}_i$ that are added back to the image tokens through a residual connection, $\tilde{\mathbf{H}}_i = \mathbf{H}_i + \Delta\mathbf{H}_i$. The resulting features $\tilde{\mathbf{H}}_i$ encode both static structure and dynamic correspondence, providing motion-consistent representations for downstream reasoning.

Global attention and target-token attention. For navigation conditioning, the sub-goal waypoint \mathcal{P}' and recent trajectory $\mathcal{P}_{t-N+1:t}$ are projected through a lightweight MLP to obtain corresponding trajectory tokens \mathbf{w} and a target token \mathbf{g} . After the tracking-guided attention, all image tokens, and trajectory tokens are passed into a unified sequence and processed jointly through multi-head self-attention layers, referred to as the *global attention* stage:

$$\mathbf{H}^{\text{global}} = \text{Attn}_{\text{global}} \left(\left[\tilde{\mathbf{H}}_{t-N+1:t}; \mathbf{w} \right] \right).$$

Subsequently, the target token \mathbf{g} is introduced and processed through another set of self-attention layers (*target-token attention*). Here we only take the updated target token $\tilde{\mathbf{g}}$ absorbing all information in past N seconds. Finally, $\tilde{\mathbf{g}}$ is passed through an MLP and two heads: an *arrival head* predicting the probability of reaching \mathcal{P}' , and an *action head* predicting the next N waypoints $\mathcal{P}_{t+1:t+N}$.

Training objectives. During training, we minimize a composite loss which is formulated as

$$\mathcal{L}_{\text{total}} = \mathcal{L}_{\text{wp}} + \lambda_{\text{arrvd}} \mathcal{L}_{\text{arrvd}} + \lambda_{\text{dir}} \mathcal{L}_{\text{dir}} \quad (1)$$

where \mathcal{L}_{wp} denotes the waypoint prediction loss measuring spatial deviation between predicted and ground-truth trajectories, $\mathcal{L}_{\text{arrvd}}$ supervises the arrival probability at the target waypoint, \mathcal{L}_{dir} compares the mean angle difference of each step. λ_{arrvd} and λ_{dir} are scalar weights balancing the auxiliary objectives. More details on these loss functions will be provided in the supplementary material.

5. Experiments

In this section, we evaluate the performance of our proposed framework, StereoWalker, for goal-directed navigation using monocular and stereo visual inputs. We aim to address the following key questions: (i) does explicitly incorporating mid-level vision features improve robot navigation over strong NFM baselines? (ii) does training with high quality stereo data enhance navigation robustness and accuracy compared to monocular setups? and (iii) does StereoWalker transfer reliably to real world robot deployments in a variety of critical navigation scenarios? To answer these questions, we outline the experimental setup, including baseline methods, evaluation metrics, and dataset collection, in Sec. 5.1. We then present stereo and monocular benchmarking results in Sec. 5.2. Finally, we provide detailed analysis of our results in Sec. 5.3.

5.1. Setup

Baselines. We compare our model with outdoor navigation models closely related to our setup, including GNM [57], ViNT [58], NoMaD [62] and CityWalker [39]. Although originally developed for image-goal navigation, we tested GNM [57], ViNT [58], and NoMaD [62] using goal-images from our collected data. We acknowledge CoNVOI [53] as a recent work with a similar setup, but could not test it due to the lack of open source code.

Evaluation Metrics. We evaluate predicted trajectories with two complementary metrics: Maximum Average orientation error (MAOE), Arrival Accuracy and Euclidean distance. Following CityWalker [39], let $\theta_{i,k}$ denote the orientation (heading) error between the predicted motion direction and the ground-truth direction for sample i at future step k . With N samples and a horizon of T steps, we define

$$\text{MAOE} = \frac{1}{N} \sum_{i=1}^N \max_{1 \leq k \leq T} \theta_{i,k}. \quad (2)$$

That is, for each sample we take the worst per-step orientation error over the horizon and then average across samples. MAOE captures the model’s ability to maintain a correct heading toward the sub-goal, independent of trajectory scale. Let $\hat{\mathbf{p}}_{i,k}$ be the predicted position for sample i at step k and \mathbf{g}_i the target waypoint. Given a radius r and a step budget K , the Arrival Accuracy is the fraction of samples that come within r of the target within the next K steps:

$$\text{Acc}_{\text{arr}}(r, K) = \frac{1}{N} \sum_{i=1}^N \mathbf{1} \left[\min_{1 \leq k \leq K} \|\hat{\mathbf{p}}_{i,k} - \mathbf{g}_i\|_2 \leq r \right]. \quad (3)$$

This metric directly reflects waypoint-level success and provides an interpretable notion of spatial goal attainment. Although Euclidean ℓ_2 distance is a straightforward measure of positional discrepancy, prior work [39] shows it can miss navigation quality, *i.e.*, trajectories may have small ℓ_2

Table 1. **Benchmark on Offline Monocular Data (CityWalker Benchmark)**. We evaluate three metrics in each critical scenario for all methods. Percentages under scenarios indicate their data proportions. The “Mean” column shows scenario means averaged over six scenarios; “All” shows sample means over all data samples. Best is **bold**; second-best is underlined.

Method	Metric	Mean	Turn	Crossing	Detour	Proximity	Crowd	Other	All
GNM [57]	↓ L2 (m)	1.22	2.36	1.36	1.42	<u>0.88</u>	<u>0.76</u>	0.55	<u>0.74</u>
	↓ MAOE (°)	16.2	31.1	14.8	12.5	14.7	12.8	11.0	12.1
	↑ Arrival (%)	68.6	66.4	69.7	66.4	69.0	69.2	70.7	70.0
ViNT [58]	↓ L2 (m)	1.30	1.91	1.13	<u>1.14</u>	0.77	0.66	<u>0.57</u>	0.70
	↓ MAOE (°)	16.5	31.1	15.4	<u>12.9</u>	14.8	13.3	11.6	12.6
	↑ Arrival (%)	70.5	71.2	68.7	70.7	73.0	68.6	71.0	70.7
NoMaD [62]	↓ L2 (m)	1.39	2.49	1.56	1.55	1.06	0.95	0.76	<u>0.74</u>
	↓ MAOE (°)	19.1	35.1	18.5	15.6	18.1	14.3	12.8	12.1
	↑ Arrival (%)	68.6	66.4	69.7	66.4	69.0	69.3	70.7	70.0
Citywalker [39]	↓ L2 (m)	1.11	1.27	1.00	1.15	1.06	1.12	1.06	1.07
	↓ MAOE (°)	<u>15.2</u>	<u>26.6</u>	<u>14.1</u>	13.9	<u>14.3</u>	<u>12.0</u>	10.4	<u>11.5</u>
	↑ Arrival (%)	<u>81.8</u>	68.9	<u>75.3</u>	78.5	90.6	87.5	90.2	87.8
StereoWalker (zero-shot)	↓ L2 (m)	<u>1.10</u>	<u>1.30</u>	1.03	1.24	1.01	1.04	0.98	1.02
	↓ MAOE (°)	15.8	26.1	14.8	17.0	14.4	12.2	<u>10.2</u>	11.7
	↑ Arrival (%)	81.0	65.3	74.9	<u>78.9</u>	86.5	<u>89.4</u>	<u>90.9</u>	<u>88.1</u>
StereoWalker	↓ L2 (m)	1.06	1.37	<u>1.01</u>	1.04	1.00	0.98	0.98	1.00
	↓ MAOE (°)	14.9	28.1	13.5	13.0	14.0	11.2	9.8	11.0
	↑ Arrival (%)	82.8	<u>70.0</u>	77.9	80.2	<u>87.3</u>	89.8	91.4	88.9

error yet head in the wrong direction. Nevertheless, ℓ_2 remains a useful indicator of absolute localization accuracy and scale, so we report it alongside MAOE and Arrival Accuracy as a complementary metric.

Data. We collected expert demonstrations through teleoperation for fine-tuning and offline evaluation. The dataset was acquired using a Clearpath Jackal equipped with an Ouster LiDAR and a ZED 2i stereo camera. A LiDAR-based SLAM system was used to estimate the robot’s pose, which served as the ground-truth action labels. Additionally, wheel odometry provided continuous relative motion estimates, enabling the robot to infer its current pose and predict its future trajectory. We also evaluated our model in a monocular setting using the CityWalker benchmark [39] in monocular settings.

5.2. Performance Benchmarking

We benchmark our model and strong baselines on the CityWalker benchmark and on our own stereo benchmark. In addition, we validate the findings with real-world navigation deployments.

Monocular Benchmark. Table 1 reports results across critical scenarios. Overall, our fine-tuned model improves performance in most categories, improving MAOE by an average of 4–13%, and arrival rates by 1–19%. Fine-tuned StereoWalker achieves the best scores on many metrics, in every scenario except the “turn” case. We hypothesize that the relative weakness on turns arises from data imbalance toward straight segments and the amplification of small ori-

Method	All	F	LT	RT
CW* [39]	50.0	57.1	42.9	50.0
Ours*	66.7	85.7	64.3	50.0
Ours [†]	73.8	85.7	71.4	64.3



Figure 4. **Real-World Navigation.** The Table shows Success rate (%) of real-world experiments in different scenarios. * and [†] indicate zero-shot inference and fine-tuned models, respectively. CW denotes CityWalker and F, LT, RT denote Forward, Left Turn, and Right Turn. The figures on the right compare StereoWalker (green) with CityWalker (yellow). Note that StereoWalker maintains a safer distance from nearby pedestrians as compared to CityWalker.

entation errors during sharp heading changes. Notably, explicitly adding mid-level vision features, including depth and tracking, improves performance on most categories, underscoring the value of structured geometric and temporal cues for monocular navigation. We provide more in depth analysis of each modality in Sec. 5.3.

Stereo Benchmark. Table 2 summarizes results across critical scenarios on our offline StereoWalker benchmark. Because our baselines do not natively ingest stereo, we feed their left image and also train a monocular variant of our model for a fair comparison. Even without stereo, our *monocular* model already yields substantial gains, reducing average L2 error by 17–73%, MAOE by 11–48%, and arrival rates by 3–24%. Training with *stereo* further achieves SOTA performance with consistent gains in *Crossing*, *Detour*, *Crowd*, and *Other*. The *Turn* scenario remains challenging, with arrival lagging behind the monocular base-

Table 2. **Benchmark on Offline StereoWalker Benchmark.** We evaluate two metrics in each critical scenario for all methods. For ViNT and Citywalker, we pass the left image as input. The “Mean” column shows scenario means averaged over six scenarios; “All” shows sample means over all data samples. Best is **bold**; second-best is underlined.

Method	Metric	Mean	Turn	Crossing	Detour	Proximity	Crowd	Other	All
GNM [57]	↓ L2 (m)	1.43	2.15	0.99	2.42	0.89	1.04	1.10	1.13
	↓ MAOE (°)	8.0	24.8	4.4	<u>5.6</u>	4.7	3.7	4.8	4.7
	↑ Arrival (%)	68.8	75.0	70.5	61.3	70.0	65.2	70.6	69.4
ViNT [58]	↓ L2 (m)	1.79	2.53	1.31	3.11	0.99	1.38	1.45	1.47
	↓ MAOE (°)	7.2	24.5	3.8	4.6	3.4	2.8	3.9	3.8
	↑ Arrival (%)	71.4	75.0	68.8	80.6	60.0	73.8	70.3	70.6
NoMaD [62]	↓ L2 (m)	2.28	2.12	2.23	2.74	2.02	2.24	2.31	2.31
	↓ MAOE (°)	9.9	26.7	6.6	9.4	5.2	5.0	6.3	6.3
	↑ Arrival (%)	72.2	66.7	68.4	71.0	80.0	75.2	72.0	71.7
CityWalker [39]	↓ L2 (m)	0.75	1.03	0.76	0.39	0.74	0.77	0.78	0.76
	↓ MAOE (°)	5.8	15.4	<u>3.4</u>	6.2	3.3	3.2	3.7	3.7
	↑ Arrival (%)	<u>83.1</u>	75.0	92.9	54.8	90.0	92.9	92.9	91.2
StereoWalker (monocular)	↓ L2 (m)	0.69	<u>1.23</u>	<u>0.66</u>	0.55	0.48	<u>0.61</u>	<u>0.63</u>	<u>0.63</u>
	↓ MAOE (°)	<u>5.4</u>	<u>14.6</u>	3.6	5.9	2.6	<u>2.3</u>	<u>3.3</u>	<u>3.3</u>
	↑ Arrival (%)	82.0	62.5	95.5	51.6	90.0	96.5	<u>95.7</u>	<u>93.7</u>
StereoWalker (stereo)	↓ L2 (m)	0.69	1.36	0.65	<u>0.42</u>	0.48	0.59	0.63	0.62
	↓ MAOE (°)	5.1	14.5	3.1	5.5	2.7	2.0	3.0	2.9
	↑ Arrival (%)	86.4	62.5	<u>93.8</u>	80.6	90.0	95.0	96.2	94.6

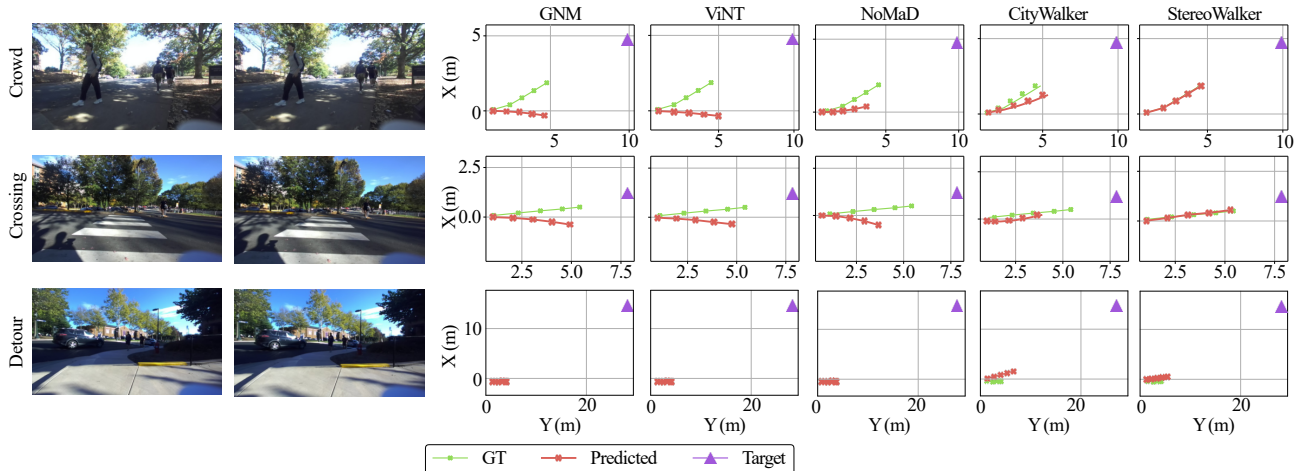


Figure 5. **Qualitative results.** We sample three trajectories from different critical scenarios in StereoWalker benchmark. In each case, the leftmost image depicts the current observation, followed by the predicted future waypoints visualized from different models.

lines despite comparable orientation error, suggesting the need for more turning-rich data or turn-aware objectives. Overall, stereo supervision provides a clear benefit beyond strong monocular baselines, reducing overall L2 error by 18–73%, MAOE by 22–54%, and arrival rates by 3–25%.

Real-world Deployment. We evaluate our model in real-world setting using a Clearpath Jackal J100 robot. The two strongest models on offline benchmarks, our model and CityWalker [39] are tested with identical start and end points to ensure comparability. Each model runs remotely on a GPU server and communicates with the robot

through FastAPI, which streams the predicted waypoints. The low-level controller on ROS2 converts the predicted short-horizon trajectory into continuous velocity commands for execution. We evaluate three motion patterns including forward, left turn, and right turn, with 14 trials conducted for each case. A trial is considered successful when the robot arrives within 1m of the designated target and stays in that area; interruptions due to collisions are marked as failures. The consistent improvements across all motion types suggests that our model architecture provides more stable waypoint estimation under dynamic conditions, and the stereo training data boosts the performance further.

Table 3. **Ablation Study.** Effect of patch tokens, depth, and dense pixel tracking on navigation performance. We report the average scenario-specific MAOE ($^{\circ}$) – lower is better.

Patch Tokens	Depth	Tracking	MAOE (\downarrow)
×	×	×	17.55
✓	×	×	16.90 (-0.65)
✓	×	✓	16.40 (-1.15)
✓	✓	×	16.23 (-1.32)
✓	✓	✓	15.77 (-1.78)

5.3. Analysis

Analysis of Mid-level Vision. Table 3 presents an ablation analysis that evaluates different architectural configurations on the CityWalker teleoperation benchmark. All variants are trained on the same monocular dataset, with specific components selectively enabled or disabled for a fair comparison. Earlier baselines such as ViNT [58], GNM [57], NoMaD [62], and CityWalker [39] represent each image using only a single [CLS] token. In contrast, we observe that using all patch tokens to capture finer spatial information leads to an immediate 3.7% improvement in the Mean Angular Orientation Error (MAOE). Building upon this representation, we observe that incorporating depth and dense pixel tracking further enhances navigation accuracy, as these two mid-level cues provide complementary inductive signals. Depth captures the three-dimensional structure, and adding depth yields a further 4.0% reduction in MAOE relative to the patch token model.

Tracking encodes scene motion and temporal consistency, and incorporating tracking on top of patch tokens and depth provides an additional 2.8% reduction in MAOE. Prior studies [9, 80] demonstrated similar advantages of mid-level vision in controlled or static environments. Our experiments in large-scale dynamic urban navigation, showing that explicitly modeling depth and motion significantly improves robustness and effectiveness in real-world conditions, shown in Fig. 4. Fine-tuned StereoWalker improves performance by an average of 23.8% over the Forward, Left turn, and Right turn scenarios. Each design takes 10 epochs and shares the same hyperparameter settings.

Analysis of Training Efficiency. Beyond performance gains, we also observe that incorporating mid-level vision capabilities significantly accelerates training. We carefully train our model on monocular data using only a fraction of the original dataset, achieving comparable performance with merely 1.5% of CityWalker’s training data. Under different amounts of training data, we use the same training settings for both CityWalker and our model. Enabling patch tokens introduces richer visual representations but also necessitates architectural modifications to the decoder, as our

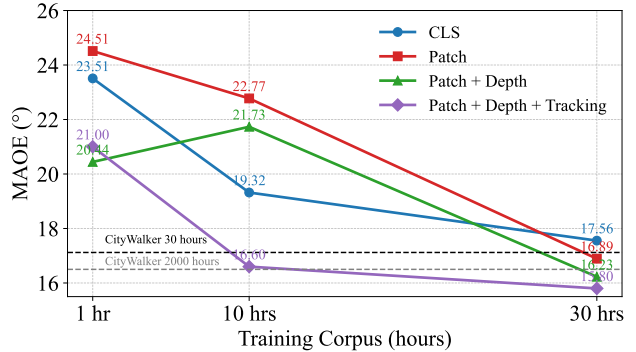


Figure 6. **Model Efficiency.** Our model empowered by *mid-level vision capabilities* can surpass 2000 hours trained CityWalker using only 30 hours data with same epochs.

model no longer relies on a single [CLS] token representation. Consequently, our model with patch tokens alone does not surpass CityWalker when trained for 30 hours. However, once depth cues are injected, the model already outperforms CityWalker. Further incorporating both depth and tracking information leads to faster convergence and superior performance, surpassing CityWalker trained with over 2,000 hours of monocular videos. This demonstrates that mid-level vision not only enhances representation quality but also provides strong inductive biases that make training more data- and time-efficient.

6. Conclusion, Limitations, and Future Work

Summary. In this work, we present a visual NFM that integrates stereo inputs with explicit mid-level vision modules for dynamic urban environments. To support this model, we collect rectified stereo videos from Internet VR180 footage, paired with an automatic filtering process. Across curated benchmarks and real-world tests, our model achieves state-of-the-art performance with remarkably training efficiency, and we analyzed the effectiveness of stereo and mid-level vision, indicating the continued relevance of core computer vision representations in the development of end-to-end robotic navigation models.

Limitations. While StereoWalker demonstrates the utility of stereo and mid-level vision for embodied navigation, these ideas are not yet fully explored across the broader landscape of robotic tasks. Many embodied systems, ranging from mobile manipulators to aerial robots, could benefit from structured geometric cues and motion-aware visual representations, yet the space of mid-level vision for general-purpose robot learning remains largely open. We view our work as an initial step toward this direction, and anticipate that future models trained on larger and more diverse multi-robot datasets may yield broader generalization and more flexible capabilities.

7. Acknowledgment

The authors acknowledge the Adobe Research Gift, the University of Virginia Research Computing and Data Analytics Center, Advanced Micro Devices AI and HPC Cluster Program, Advanced Cyberinfrastructure Coordination Ecosystem: Services & Support (ACCESS) program, and National Artificial Intelligence Research Resource (NAIRR) Pilot for computational resources, including the Anvil supercomputer (National Science Foundation award OAC 2005632) at Purdue University and the Delta and DeltaAI advanced computing resources (National Science Foundation award OAC 2005572). PI Chandra is supported in part by a CCI award supported by the Commonwealth of Virginia.

References

- [1] Ziad Al-Halah, Santhosh Kumar Ramakrishnan, and Kristen Grauman. Zero experience required: Plug & play modular transfer learning for semantic visual navigation. In *Proceedings of the IEEE/CVF Conference on Computer Vision and Pattern Recognition*, pages 17031–17041, 2022. 2
- [2] Kaixin Bai, Huajian Zeng, Lei Zhang, Yiwen Liu, Hongli Xu, Zhaopeng Chen, and Jianwei Zhang. Cleardepth: enhanced stereo perception of transparent objects for robotic manipulation. *arXiv preprint arXiv:2409.08926*, 2024. 2
- [3] Grzegorz Bartyzel, Wojciech Pólchłópek, and Dominik Rzepka. Reinforcement learning with stereo-view observation for robust electronic component robotic insertion. *Journal of Intelligent & Robotic Systems*, 109(3):57, 2023. 2
- [4] Angel Chang, Angela Dai, Thomas Funkhouser, Maciej Halber, Matthias Niessner, Manolis Savva, Shuran Song, Andy Zeng, and Yinda Zhang. Matterport3d: Learning from RGB-D data in indoor environments. *3DV*, 2017. 2
- [5] Matthew Chang, Arjun Gupta, and Saurabh Gupta. Semantic visual navigation by watching youtube videos. *Advances in Neural Information Processing Systems*, 33:4283–4294, 2020. 2
- [6] Devendra Singh Chaplot, Dhiraj Gandhi, Saurabh Gupta, Abhinav Gupta, and Ruslan Salakhutdinov. Learning to explore using active neural slam. In *International Conference on Learning Representations (ICLR)*, 2020. 2
- [7] Devendra Singh Chaplot, Dhiraj Prakashchand Gandhi, Abhinav Gupta, and Russ R Salakhutdinov. Object goal navigation using goal-oriented semantic exploration. *NeurIPS*, 33: 4247–4258, 2020. 2
- [8] Prithvijit Chattopadhyay, Judy Hoffman, Roozbeh Mottaghi, and Aniruddha Kembhavi. Robustnav: Towards benchmarking robustness in embodied navigation. In *Proceedings of the IEEE/CVF International Conference on Computer Vision*, pages 15691–15700, 2021. 2
- [9] Bryan Chen, Alexander Sax, Francis Lewis, Iro Armeni, Silvio Savarese, Amir Zamir, Jitendra Malik, and Lerrel Pinto. Robust policies via mid-level visual representations: An experimental study in manipulation and navigation. In *Proceedings of the 2020 Conference on Robot Learning*, pages 2328–2346. PMLR, 2021. 2, 8
- [10] Jeffrey Chen and Rohan Chandra. Livepoint: Fully decentralized, safe, deadlock-free multi-robot control in cluttered environments with high-dimensional inputs. *arXiv preprint arXiv:2503.13098*, 2025. 2
- [11] Yutao Chen, Yahao Wang, Xuming Tang, Kai Wu, Shaolei Wu, Rui Guo, Yu Feng, and Erbao Dong. Intelligent power distribution live-line operation robot systems based on stereo camera. *High Voltage*, 8(6):1306–1318, 2023. 2
- [12] Junda Cheng, Longliang Liu, Gangwei Xu, Xianqi Wang, Zhaoxing Zhang, Yong Deng, Jinliang Zang, Yurui Chen, Zhipeng Cai, and Xin Yang. Monster: Marry monodepth to stereo unleashes power. In *Proceedings of the Computer Vision and Pattern Recognition Conference*, pages 6273–6282, 2025. 4, 1, 2
- [13] Xuxin Cheng, Jialong Li, Shiqi Yang, Ge Yang, and Xiaolong Wang. Open-television: Teleoperation with immersive active visual feedback. In *8th Annual Conference on Robot Learning*, 2024. 2
- [14] Samuel Clarke, Suzannah Wistreich, Yanjie Ze, and Jiajun Wu. X-capture: An open-source portable device for multi-sensory learning. In *Proceedings of the IEEE/CVF International Conference on Computer Vision (ICCV)*, pages 6436–6446, 2025. 2
- [15] Abhishek Das, Samyak Datta, Georgia Gkioxari, Stefan Lee, Devi Parikh, and Dhruv Batra. Embodied question answering. In *CVPR*, pages 1–10, 2018. 2
- [16] Massimiliano De Sa, Prasanth Kotaru, and Koushil Sreenath. Point cloud-based control barrier function regression for safe and efficient vision-based control. In *2024 IEEE International Conference on Robotics and Automation (ICRA)*, pages 366–372. IEEE, 2024. 2
- [17] Guillermo Gallego, Henri Rebecq, and Davide Scaramuzza. A unifying contrast maximization framework for event cameras, with applications to motion, depth, and optical flow estimation. In *Proceedings of the IEEE conference on computer vision and pattern recognition*, pages 3867–3876, 2018. 2
- [18] Theophile Gervet, Soumith Chintala, Dhruv Batra, Jitendra Malik, and Devendra Singh Chaplot. Navigating to objects in the real world. *Science Robotics*, 8(79):eadf6991, 2023. 2
- [19] Daniel Gordon, Abhishek Kadian, Devi Parikh, Judy Hoffman, and Dhruv Batra. Splitnet: Sim2sim and task2task transfer for embodied visual navigation. In *Proceedings of the IEEE/CVF International Conference on Computer Vision*, pages 1022–1031, 2019. 2
- [20] Tianrui Guan, Divya Kothandaraman, Rohan Chandra, Adarsh Jagan Sathyamoorthy, Kasun Weerakoon, and Dinesh Manocha. Ga-nav: Efficient terrain segmentation for robot navigation in unstructured outdoor environments. *IEEE Robotics and Automation Letters*, 7(3):8138–8145, 2022. 1
- [21] Saurabh Gupta, James Davidson, Sergey Levine, Rahul Sukthankar, and Jitendra Malik. Cognitive mapping and planning for visual navigation. In *CVPR*, pages 2616–2625, 2017. 2

- [22] Meera Hahn, Devendra Singh Chaplot, Shubham Tulsiani, Mustafa Mukadam, James M Rehg, and Abhinav Gupta. No rl, no simulation: Learning to navigate without navigating. *NeurIPS*, 34:26661–26673, 2021. 2
- [23] Botao He, Ze Wang, Yuan Zhou, Jingxi Chen, Chahat Deep Singh, Haojia Li, Yuman Gao, Shaojie Shen, Kaiwei Wang, Yanjun Cao, et al. Microsaccade-inspired event camera for robotics. *Science Robotics*, 9(90):eadj8124, 2024. 2
- [24] Honglin He, Yukai Ma, Wayne Wu, and Bolei Zhou. From seeing to experiencing: Scaling navigation foundation models with reinforcement learning. *arXiv preprint arXiv:2507.22028*, 2025. 2
- [25] Max Jaderberg, Volodymyr Mnih, Wojciech Marian Czarnecki, Tom Schaul, Joel Z Leibo, David Silver, and Koray Kavukcuoglu. Reinforcement learning with unsupervised auxiliary tasks. In *ICLR*, 2017. 2
- [26] Bo Jiang, Shaoyu Chen, Qing Xu, Bencheng Liao, Jiajie Chen, Helong Zhou, Qian Zhang, Wenyu Liu, Chang Huang, and Xinggang Wang. Vad: Vectorized scene representation for efficient autonomous driving. In *Proceedings of the IEEE/CVF International Conference on Computer Vision*, pages 8340–8350, 2023. 2
- [27] Linyi Jin, Richard Tucker, Zhengqi Li, David Fouhey, Noah Snavely, and Aleksander Holynski. Stereo4D: Learning How Things Move in 3D from Internet Stereo Videos. In *Proceedings of the IEEE/CVF Conference on Computer Vision and Pattern Recognition*, 2025. 3, 1
- [28] Nikita Karaev, Yuri Makarov, Jianyuan Wang, Natalia Neverova, Andrea Vedaldi, and Christian Rupprecht. Co-tracker3: Simpler and better point tracking by pseudo-labelling real videos. In *Proceedings of the IEEE/CVF International Conference on Computer Vision*, pages 6013–6022, 2025. 4, 1, 2
- [29] Alexander Khazatsky, Karl Pertsch, Suraj Nair, Ashwin Balakrishna, Sudeep Dasari, Siddharth Karamcheti, Soroush Nasiriany, Mohan Kumar Srirama, Lawrence Yunliang Chen, Kirsty Ellis, Peter David Fagan, Joey Hejna, Masha Itkina, Marion Lepert, Yecheng Jason Ma, Patrick Tree Miller, Jimmy Wu, Suneel Belkhale, Shivin Dass, Huy Ha, Arhan Jain, Abraham Lee, Youngwoon Lee, Marius Memmel, Sungjae Park, Ilija Radosavovic, Kaiyuan Wang, Albert Zhan, Kevin Black, Cheng Chi, Kyle Beltran Hatch, Shan Lin, Jingpei Lu, Jean Mercat, Abdul Rehman, Pannag R Sanketi, Archit Sharma, Cody Simpson, Quan Vuong, Homer Rich Walke, Blake Wulfe, Ted Xiao, Jonathan Heewon Yang, Arefeh Yavary, Tony Z. Zhao, Christopher Agia, Rohan Baijal, Mateo Guaman Castro, Daphne Chen, Qiuyu Chen, Trinity Chung, Jaimyn Drake, Ethan Paul Foster, Jensen Gao, Vitor Guizilini, David Antonio Herrera, Minh Heo, Kyle Hsu, Jiaheng Hu, Muhammad Zubair Irshad, Donovan Jackson, Charlotte Le, Yunshuang Li, Kevin Lin, Roy Lin, Zehan Ma, Abhiram Maddukuri, Suvir Mirchandani, Daniel Morton, Tony Nguyen, Abigail O’Neill, Rosario Scalise, Derick Seale, Victor Son, Stephen Tian, Emi Tran, Andrew E. Wang, Yilin Wu, Annie Xie, Jingyun Yang, Patrick Yin, Yunchu Zhang, Osbert Bastani, Glen Berseth, Jeannette Bohg, Ken Goldberg, Abhinav Gupta, Abhishek Gupta, Dinesh Jayaraman, Joseph J Lim, Jitendra Malik, Roberto Martín-Martín, Subramanian Ramamoorthy, Dorsa Sadigh, Shuran Song, Jiajun Wu, Michael C. Yip, Yuke Zhu, Thomas Kollar, Sergey Levine, and Chelsea Finn. Droid: A large-scale in-the-wild robot manipulation dataset. 2024. 2
- [30] J Zico Kolter, Youngjun Kim, and Andrew Y Ng. Stereo vision and terrain modeling for quadruped robots. In *2009 IEEE International Conference on Robotics and Automation*, pages 1557–1564. IEEE, 2009. 2
- [31] Eric Kolve, Roozbeh Mottaghi, Winson Han, Eli VanderBilt, Luca Weihs, Alvaro Herrasti, Matt Deitke, Kiana Ehsani, Daniel Gordon, Yuke Zhu, et al. Ai2-thor: An interactive 3d environment for visual ai. *arXiv preprint arXiv:1712.05474*, 2017. 2
- [32] Jacob Krantz, Erik Wijmans, Arjun Majumdar, Dhruv Batra, and Stefan Lee. Beyond the nav-graph: Vision-and-language navigation in continuous environments. In *ECCV*, pages 104–120. Springer, 2020. 2
- [33] Jacob Krantz, Theophile Gervet, Karmesh Yadav, Austin Wang, Chris Paxton, Roozbeh Mottaghi, Dhruv Batra, Jitendra Malik, Stefan Lee, and Devendra Singh Chaplot. Navigating to objects specified by images. In *CVPR*, pages 10916–10925, 2023. 2
- [34] Rainer Kümmerle, Michael Ruhnke, Bastian Steder, Cyrill Stachniss, and Wolfram Burgard. A navigation system for robots operating in crowded urban environments. In *ICRA*, pages 3225–3232. IEEE, 2013. 1
- [35] Obin Kwon, Nuri Kim, Yunho Choi, Hwiyeon Yoo, Jeongho Park, and Songhwai Oh. Visual graph memory with unsupervised representation for visual navigation. In *CVPR*, pages 15890–15899, 2021. 2
- [36] Zihang Lai and Andrea Vedaldi. Tracktention: Leveraging point tracking to attend videos faster and better. In *Proceedings of the Computer Vision and Pattern Recognition Conference*, pages 22809–22819, 2025. 4, 1
- [37] Jialong Li, Xuxin Cheng, Tianshu Huang, Shiqi Yang, Ri-Zhao Qiu, and Xiaolong Wang. Amo: Adaptive motion optimization for hyper-dexterous humanoid whole-body control. *arXiv preprint arXiv:2505.03738*, 2025. 2
- [38] Zhiqi Li, Wenhai Wang, Hongyang Li, Enze Xie, Chonghao Sima, Tong Lu, Qiao Yu, and Jifeng Dai. Bevformer: learning bird’s-eye-view representation from lidar-camera via spatiotemporal transformers. *IEEE Transactions on Pattern Analysis and Machine Intelligence*, 2024. 2
- [39] Xinhao Liu, Jintong Li, Yicheng Jiang, Niranjan Sujay, Zhicheng Yang, Juexiao Zhang, John Abanes, Jing Zhang, and Chen Feng. Citywalker: Learning embodied urban navigation from web-scale videos. In *Proceedings of the Computer Vision and Pattern Recognition Conference*, pages 6875–6885, 2025. 2, 3, 5, 6, 7, 8, 1
- [40] Ilya Loshchilov and Frank Hutter. Decoupled weight decay regularization. In *International Conference on Learning Representations*, 2019. 2
- [41] Zheng Ma, Xiaoguang Hu, and Yulin Zhou. Cross-shaped peg-in-hole autonomous assembly system via bp neural network based on force/moment and visual information. *Machine*, 12(12):846, 2024. 2

- [42] Arjun Majumdar, Gunjan Aggarwal, Bhavika Devnani, Judy Hoffman, and Dhruv Batra. Zson: Zero-shot object-goal navigation using multimodal goal embeddings. *NeurIPS*, 35: 32340–32352, 2022. [2](#)
- [43] Lina Mezghan, Sainbayar Sukhbaatar, Thibaut Lavril, Oleksandr Maksymets, Dhruv Batra, Piotr Bojanowski, and Karteek Alahari. Memory-augmented reinforcement learning for image-goal navigation. In *2022 IEEE/RSJ International Conference on Intelligent Robots and Systems (IROS)*, pages 3316–3323. IEEE, 2022. [2](#)
- [44] Yoichi Morales, Alexander Carballo, Eijiro Takeuchi, Atsushi Aburadani, and Takashi Tsubouchi. Autonomous robot navigation in outdoor cluttered pedestrian walkways. *Journal of Field Robotics*, 26(8):609–635, 2009. [1](#)
- [45] Arsalan Mousavian, Alexander Toshev, Marek Fišer, Jana Košecá, Ayzaan Wahid, and James Davidson. Visual representations for semantic target driven navigation. In *2019 International Conference on Robotics and Automation (ICRA)*, pages 8846–8852. IEEE, 2019. [2](#)
- [46] Matthias Mueller, Alexey Dosovitskiy, Bernard Ghanem, and Vladlen Koltun. Driving policy transfer via modularity and abstraction. In *Proceedings of The 2nd Conference on Robot Learning*, pages 1–15. PMLR, 2018. [2](#)
- [47] Quirin Muhlbauer, Stefan Sosnowski, Tingting Xu, Tianguang Zhang, Kolja Kuhnlenz, and Martin Buss. Navigation through urban environments by visual perception and interaction. In *ICRA*, pages 3558–3564. IEEE, 2009. [1](#)
- [48] Maxime Oquab, Timothée Darcet, Théo Moutakanni, Huy V. Vo, Marc Szafraniec, Vasil Khalidov, Pierre Fernandez, Daniel HAZIZA, Francisco Massa, Alaaeldin El-Nouby, Mido Assran, Nicolas Ballas, Wojciech Galuba, Russell Howes, Po-Yao Huang, Shang-Wen Li, Ishan Misra, Michael Rabbat, Vasu Sharma, Gabriel Synnaeve, Hu Xu, Herve Jegou, Julien Mairal, Patrick Labatut, Armand Joulin, and Piotr Bojanowski. DINOv2: Learning robust visual features without supervision. *Transactions on Machine Learning Research*, 2024. [4](#), [2](#)
- [49] Zhangyang Qi, Zhixiong Zhang, Yizhou Yu, Jiaqi Wang, and Hengshuang Zhao. Vln-r1: Vision-language navigation via reinforcement fine-tuning. *arXiv preprint arXiv:2506.17221*, 2025. [2](#)
- [50] Yuheng Qiu, Yutian Chen, Zihao Zhang, Wenshan Wang, and Sebastian Scherer. Mac-vo: Metrics-aware covariance for learning-based stereo visual odometry mac-vo. github. io. In *2025 IEEE International Conference on Robotics and Automation (ICRA)*, pages 3803–3814. IEEE, 2025. [3](#)
- [51] Santhosh Kumar Ramakrishnan, Devendra Singh Chaplot, Ziad Al-Halah, Jitendra Malik, and Kristen Grauman. Poni: Potential functions for objectgoal navigation with interaction-free learning. In *Proceedings of the IEEE/CVF Conference on Computer Vision and Pattern Recognition*, pages 18890–18900, 2022. [2](#)
- [52] Hazem Rashed, Mohamed Ramzy, Victor Vaquero, Ahmad El Sallab, Ganesh Sistu, and Senthil Yogamani. Fusemodnet: Real-time camera and lidar based moving object detection for robust low-light autonomous driving. In *Proceedings of the IEEE/CVF international conference on computer vision workshops*, pages 0–0, 2019. [2](#)
- [53] Adarsh Jagan Sathyamoorthy, Kasun Weerakoon, Mohamed Elnoor, Anuj Zore, Brian Ichter, Fei Xia, Jie Tan, Wenhao Yu, and Dinesh Manocha. Convoi: Context-aware navigation using vision language models in outdoor and indoor environments. In *2024 IEEE/RSJ International Conference on Intelligent Robots and Systems (IROS)*, pages 13837–13844. IEEE, 2024. [5](#)
- [54] Nikolay Savinov, Alexey Dosovitskiy, and Vladlen Koltun. Semi-parametric topological memory for navigation. In *ICLR*, 2018. [2](#)
- [55] Manolis Savva, Abhishek Kadian, Oleksandr Maksymets, Yili Zhao, Erik Wijmans, Bhavana Jain, Julian Straub, Jia Liu, Vladlen Koltun, Jitendra Malik, et al. Habitat: A platform for embodied ai research. In *CVPR*, pages 9339–9347, 2019. [2](#)
- [56] Alexander Sax, Jeffrey O. Zhang, Bradley Emi, Amir Zamir, Silvio Savarese, Leonidas Guibas, and Jitendra Malik. Learning to navigate using mid-level visual priors. In *Proceedings of the Conference on Robot Learning*, pages 791–812. PMLR, 2020. [2](#)
- [57] Dhruv Shah, Ajay Sridhar, Arjun Bhorkar, Noriaki Hirose, and Sergey Levine. Gnm: A general navigation model to drive any robot. In *ICRA*, pages 7226–7233. IEEE, 2023. [2](#), [3](#), [5](#), [6](#), [7](#), [8](#)
- [58] Dhruv Shah, Ajay Sridhar, Nitish Dashora, Kyle Stachowicz, Kevin Black, Noriaki Hirose, and Sergey Levine. ViNT: A foundation model for visual navigation. In *CoRL*, 2023. [2](#), [3](#), [5](#), [6](#), [7](#), [8](#)
- [59] Krishna Shankar, Mark Tjersland, Jeremy Ma, Kevin Stone, and Max Bajracharya. A learned stereo depth system for robotic manipulation in homes. *IEEE Robotics and Automation Letters*, 7(2):2305–2312, 2022. [2](#)
- [60] Jun Shi, A Yong, Yixiang Jin, Dingzhe Li, Haoyu Niu, Zhezhu Jin, and He Wang. Asgrasp: Generalizable transparent object reconstruction and 6-dof grasp detection from rgb-d active stereo camera. In *2024 IEEE international conference on robotics and automation (ICRA)*, pages 5441–5447. IEEE, 2024. [2](#)
- [61] Oren Spector, Vladimir Tchuiev, and Dotan Di Castro. Insertionnet 2.0: Minimal contact multi-step insertion using multimodal multiview sensory input. In *2022 International Conference on Robotics and Automation (ICRA)*, pages 6330–6336. IEEE, 2022. [2](#)
- [62] Ajay Sridhar, Dhruv Shah, Catherine Glossop, and Sergey Levine. Nomad: Goal masked diffusion policies for navigation and exploration. In *ICRA*, pages 63–70, 2024. [2](#), [3](#), [5](#), [6](#), [7](#), [8](#)
- [63] Hao Tan, Licheng Yu, and Mohit Bansal. Learning to navigate unseen environments: Back translation with environmental dropout. In *Proceedings of the 2019 Conference of the North American Chapter of the Association for Computational Linguistics: Human Language Technologies, Volume 1 (Long and Short Papers)*, pages 2610–2621, Minneapolis, Minnesota, 2019. Association for Computational Linguistics. [2](#)
- [64] Zachary Teed, Lahav Lipson, and Jia Deng. Deep patch visual odometry. *NeurIPS*, 36, 2024. [3](#)

- [65] Peng Wang, Shuai Bai, Sinan Tan, Shijie Wang, Zhihao Fan, Jinze Bai, Keqin Chen, Xuejing Liu, Jialin Wang, Wenbin Ge, et al. Qwen2-vl: Enhancing vision-language model’s perception of the world at any resolution. *arXiv preprint arXiv:2409.12191*, 2024. [3](#), [1](#)
- [66] Erik Wijmans, Abhishek Kadian, Ari S. Morcos, Stefan Lee, Irfan Essa, Devi Parikh, Manolis Savva, and Dhruv Batra. Dd-ppo: Learning near-perfect pointgoal navigators from 2.5 billion frames. In *ICLR*, 2019. [2](#)
- [67] Wayne Wu, Honglin He, Jack He, Yiran Wang, Chenda Duan, Zhizheng Liu, Quanyi Li, and Bolei Zhou. Metaurban: An embodied ai simulation platform for urban micromobility. *International Conference on Learning Representation*, 2025. [2](#)
- [68] Wayne Wu, Honglin He, Chaoyuan Zhang, Jack He, Seth Z. Zhao, Ran Gong, Quanyi Li, and Bolei Zhou. Towards autonomous micromobility through scalable urban simulation. In *Proceedings of the IEEE/CVF Conference on Computer Vision and Pattern Recognition*, 2025.
- [69] Fei Xia, Amir R Zamir, Zhiyang He, Alexander Sax, Jitendra Malik, and Silvio Savarese. Gibson env: Real-world perception for embodied agents. In *CVPR*, pages 9068–9079, 2018.
- [70] Ziyang Xie, Zhizheng Liu, Zhenghao Peng, Wayne Wu, and Bolei Zhou. Vid2sim: Realistic and interactive simulation from video for urban navigation. *CVPR*, 2025. [2](#)
- [71] Zhefan Xu, Haoyu Shen, Xinming Han, Hanyu Jin, Kanlong Ye, and Kenji Shimada. Lv-dot: Lidar-visual dynamic obstacle detection and tracking for autonomous robot navigation. *arXiv preprint arXiv:2502.20607*, 2025. [2](#)
- [72] Lihe Yang, Bingyi Kang, Zilong Huang, Zhen Zhao, Xiaogang Xu, Jiashi Feng, and Hengshuang Zhao. Depth anything v2. *Advances in Neural Information Processing Systems*, 37:21875–21911, 2024. [4](#), [1](#), [2](#)
- [73] Wei Yang, Xiaolong Wang, Ali Farhadi, Abhinav Gupta, and Roozbeh Mottaghi. Visual semantic navigation using scene priors. *arXiv preprint arXiv:1810.06543*, 2018. [2](#)
- [74] Jin Yao, Hao Gu, Xuweiyi Chen, Jiayun Wang, and Zezhou Cheng. Open vocabulary monocular 3d object detection, 2024.
- [75] Jin Yao, Radowan Mahmud Redoy, Sebastian Elbaum, Matthew B. Dwyer, and Zezhou Cheng. Labelany3d: Label any object 3d in the wild. In *Neural Information Processing Systems (NeurIPS)*, 2025.
- [76] Lin Yen-Chen, Andy Zeng, Shuran Song, Phillip Isola, and Tsung-Yi Lin. Learning to see before learning to act: Visual pre-training for manipulation. In *2020 IEEE International Conference on Robotics and Automation (ICRA)*, pages 7286–7293. IEEE, 2020. [2](#)
- [77] Shaofeng Yin, Yanjie Ze, Hong-Xing Yu, C Karen Liu, and Jiajun Wu. Visualmimic: Visual humanoid locomanipulation via motion tracking and generation. *arXiv preprint arXiv:2509.20322*, 2025. [2](#)
- [78] Jiazhao Zhang, Kunyu Wang, Shaoan Wang, Minghan Li, Haoran Liu, Songlin Wei, Zhongyuan Wang, Zhizheng Zhang, and He Wang. Uni-navid: A video-based vision-language-action model for unifying embodied navigation tasks. *arXiv preprint arXiv:2412.06224*, 2024. [2](#)
- [79] Jiazhao Zhang, Kunyu Wang, Rongtao Xu, Gengze Zhou, Yicong Hong, Xiaomeng Fang, Qi Wu, Zhizheng Zhang, and He Wang. Navid: Video-based vlm plans the next step for vision-and-language navigation. *arXiv preprint arXiv:2402.15852*, 2024. [2](#)
- [80] Brady Zhou, Philipp Krähenbühl, and Vladlen Koltun. Does computer vision matter for action? *Science Robotics*, 4(30): eaaw6661, 2019. [2](#), [8](#)
- [81] Zhiguo Zhou, Xin Feng, Shunfan Di, and Xuehua Zhou. A lidar mapping system for robot navigation in dynamic environments. *IEEE Transactions on Intelligent Vehicles*, 2023. [2](#)
- [82] Yuke Zhu, Roozbeh Mottaghi, Eric Kolve, Joseph J Lim, Abhinav Gupta, Li Fei-Fei, and Ali Farhadi. Target-driven visual navigation in indoor scenes using deep reinforcement learning. In *2017 IEEE international conference on robotics and automation (ICRA)*, pages 3357–3364. IEEE, 2017. [2](#)

Empowering Dynamic Urban Navigation with Stereo and Mid-Level Vision

Supplementary Material

Sec. A reports the evaluation metrics and provides detailed statistics of the DIVERCITY dataset. Sec. B presents additional training details for StereoWalker, including the full set of hyperparameters, our implementation of the tracking-guided attention module, as the original Tracktention work [36] did not release source code, and an extended ablation study. Sec. C further describes real-world deployment settings and includes supplementary qualitative visualizations.

A. DIVERCITY Data Curation

For the collection of stereo walking videos, we curate footage captured across multiple cities, extending beyond prior datasets such as CityWalker [39], which its data is curated on videos from a single creator and limited to New York City. All videos are downloaded in VR180 format and subsequently rectified using the pipeline provided by Stereo4D [27], producing synchronized left and right perspective views at a resolution of 350×350 and a frame rate of 30 fps. Moreover, CityWalker contains non-navigation content as shown in Fig. 7. For example, the creator will stop and watch events and etc. To remove such noisy from our dataset, we adopt Qwen2-VL [65] to filter all the videos collected using the prompt: “*Is this a first-person video of a person actively walking on foot (not standing still)? Answer strictly with ‘yes’ or ‘no’.*” Based on the feedback from Qwen2-VL [65], we filter out clips with the answer of ‘no’. As a result, 544 of 748 video clips are selected as valid navigation clips. In addition, we verify the process of filtering by hand annotating 100 video clips and obtained a precision of 100% and a recall of 97.5%, which demonstrate the reliability and effectiveness of this video filtering strategy.

For additional quality control and action label acquisition, please refer to Sec. 3.

B. Experimental Details

In this section, we introduce details of StereoWalker. Sec. B.1 provides detailed settings used in training; Sec. B.2 demonstrates the complete process of tracking-guided attention; Sec. B.3 gives the performance in all subsets of the benchmark for ablation study.

B.1. More Training Details

We train StereoWalker under the hyperparameter settings summarized in Tab. 4. The model is optimized for ten epochs using AdamW with an initial learning rate of 2×10^{-4} and a cosine decay schedule, and a reduced learning rate of 5×10^{-5} during fine-tuning. Training is conducted



Figure 7. **Distracting scenes.** The CityWalker videos include non-navigation content, resulting in noise that undermines reliable navigation learning. We filter out such clips using our data filtering approach.

on four NVIDIA A100 GPUs with 80GB memory, resulting in a total wall-clock time of approximately five hours.

For the mid-level vision components, we adopt lightweight and fast-inference variants of state-of-the-art models to balance computational efficiency and representational quality. Specifically, RT-MonSter++ [12] is used as the binocular depth estimator to produce high-quality disparity and depth maps from stereo inputs, while CoTracker3 online [28] is applied for point tracking to provide temporally coherent motion cues across frames. For monocular depth estimation, we employ Depth-Anything-V2-Base [72], which directly operates on hierarchical features extracted from DINOv2 with a ViT-B/14 backbone with feature dimension of 768.

All inputs are resized to a resolution of 350×350 . While the depth embedding dimension is 64. These are concatenated with DINO feature to form image tokens with an attention hidden dimension of 832. The network comprises two tracking-guided attention layers, twelve global attention layers, and four target-token attention layers. Each training sample uses a temporal context of five past frames and predicts five future waypoints at a frequency of 1 Hz, along with an arrival probability.

The loss function weights are set to $\lambda_{\text{arrvd}} = 1.0$ and $\lambda_{\text{dir}} = 10.0$. Empirically, we find this hyperparameter provides better directional consistency in critical scenarios.

B.2. Implementation of Tracking-guided Attention

Although our tracking-guided attention is inspired by Tracktention [36], their code has not yet released. We now provide the details of our design of this module and will public the implementation for reproducing our results.

Following Tracktention [36], let j, k be the patch

Hyperparameter	Value
Model	
Total # Parameters	334M
Trainable # Parameters	168M
Image Encoder	DINOv2 [48]
Depth Estimator (Monocular)	Depth-Anything-V2-Base [72]
Depth Estimator (Binocular)	RT-MonSter++ [12]
Point Tracker	CoTracker3 online [28]
Backbone Arch.	ViT-B/14
Input Resolution	350 × 350
Dino Feature Dimension	768
Depth Embedding Dimension	64
Attn. Hidden Dim.	832
# Tracking-guided Attention Layers	2
# Global Attention Layers	12
# Target-token Attention Layer	4
Input Context	5
Predicted Waypoints	5
Image & Past Trajectory Frequency	1 Hz
Training	
# Epochs	10
Batch Size	48
Learning Rate	2×10^{-4}
Optimizer	AdamW [40]
LR Schedule	Cosine
Compute Resources	4 × A100 80GB
Training Walltime	5 hours
Fine-tuning LR	5×10^{-5}
λ_{arrvd}	1.0
λ_{dir}	10.0

Table 4. Hyperparameters for training the StereoWalker model.

position in an image, H, W be the height and width of the patchified image. For one patch, $\mathbf{x}_{j,k}$ denotes DINO-derived appearance embedding, and $\mathbf{z}_{j,k}$ denote depth embedding. We then get patch tokens $\mathbf{h}_{j,k} = [\mathbf{x}_{j,k}; \mathbf{z}_{j,k}] \in \mathbb{R}^d$ that concatenates these two embeddings. Tracking-guided attention takes as input the tokens $\mathbf{H}_i = \{\mathbf{h}_{1:H,1:W}\}_i$ for each frame i in the window $t-k+1, \dots, t$, and a set of point tracks $\mathbf{T}_i^{\text{trk}} = \{\mathbf{p}_{i,m} \in \mathbb{R}^2\}_{m=1}^{M_{\text{trk}}}$ produced by the point tracker, where M_{trk} is the number of tracks.

We first convert the 2D track positions $\mathbf{p}_{i,m}$ into track tokens by applying a 2D RoPE with regard to its patch position and a linear projection W_T ,

$$\mathbf{q}_{i,m}^{\text{trk}} = W_T \text{RoPE}(\mathbf{p}_{i,m}) \in \mathbb{R}^d,$$

and arrange them into a tensor $\mathbf{Q}_i^{\text{trk}} \in \mathbb{R}^{M_{\text{trk}} \times d}$. The image tokens for frame i are stacked as $\mathbf{H}_i \in \mathbb{R}^{HW \times d}$ and also applied RoPE on. We then use cross-attention to pool information from image tokens into the track tokens,

$$\mathbf{S}_i = \text{Attn}(\mathbf{Q}_i^{\text{trk}} \mathbf{W}_Q, \mathbf{H}_i \mathbf{W}_K, \mathbf{H}_i \mathbf{W}_V),$$

where $\mathbf{S}_i \in \mathbb{R}^{M_{\text{trk}} \times d}$ are track features that summarize the local neighborhood of each track in the feature map. Intuitively, this stage samples feature information around each track location using a learnable, attention-based weighting rather than fixed interpolation.

To aggregate information over time, we apply a transformer along the temporal dimension of each track. Let $\mathbf{S}_{1:k} = \{\mathbf{S}_i\}_{i=1}^k \in \mathbb{R}^{k \times M_{\text{trk}} \times d}$ denote all track features in the window, which we rearrange into a tensor of shape $M_{\text{trk}} \times k \times d$ by treating each track as a short sequence in time. A track transformer \mathcal{T}_{trk} is applied independently to each track sequence,

$$\tilde{\mathbf{S}} = \mathcal{T}_{\text{trk}}(\mathbf{S}_{1:T}),$$

yielding updated track tokens $\tilde{\mathbf{S}}_{i,m}$ that carry temporally smoothed information along the corresponding trajectories.

In the final stage, we redistribute the updated track features back to the image token grid. We construct queries from spatial coordinate embeddings $\mathbf{c}_{j,k}$ associated with each image token $\mathbf{h}_{j,k}$ and use the updated track tokens as keys and values,

$$\text{Attn}(\mathbf{C}_i \mathbf{W}'_Q, \tilde{\mathbf{S}}_i \mathbf{W}'_K, \tilde{\mathbf{S}}_i \mathbf{W}'_V),$$

where $\mathbf{C}_i = \{\mathbf{c}_{j,k}\}_{j=1}^M$ and the output encodes motion-aware corrections for each image token. As a result, the final tokens incorporate both local appearance and trajectory-aligned motion information, while preserving the spatial layout of the original feature map.

Different from Tracktention paper, which alternates ViT and Tracktention blocks multiple times, we employ only two tracking-guided attention layers at the beginning of the transformer for efficiency, since we are approaching from the robotics side.

B.3. More Ablation Details

In Tab. 5, we report the performance of different architectural variants across all evaluation scenarios. The full StereoWalker model achieves the best MAOE on average and overall. We observe that replacing the CLS token with dense patch tokens and introducing mid-level vision modules consistently improves performance across most settings, indicating their effectiveness in enhancing waypoint prediction quality. Specifically, the addition of depth and tracking improves performance to different extents across scenarios, further illustrating the complementary inductive information contributed by these components.

We also observe that in the *Detour* scenario, where a slight performance drop is observed. As also discussed in CityWalker, this subset of the benchmark contains a relatively small number of samples, making the results more sensitive to data imbalance. Notably, both CityWalker and our model exhibit substantial gains after fine-tuning on this scenario, with CityWalker improving from 16.3 to 13.9 MAOE and our model from 17.0 to 13.0, suggesting that increased data or targeted fine-tuning can significantly mitigate this limitation.

Patch Tokens	Depth	Tracking	Mean	Turn	Crossing	Detour	Proximity	Crowd	Other	All
			17.56	31.39	16.12	14.70	17.68	13.01	12.44	13.60
✓			16.89	31.47	15.65	13.65	15.85	13.12	11.60	12.78
✓		✓	16.40	27.89	15.10	17.77	14.83	12.54	10.24	11.84
✓	✓		16.23	26.24	15.48	18.61	14.25	12.57	10.22	11.86
✓	✓	✓	15.77	26.08	14.79	17.03	14.38	12.16	10.19	11.68

Table 5. **Full Ablation Study.** Here we provide an extended ablation study in supplementary Tab. 3. The result is evaluated for all scenarios.

C. Real-world Deployment Details

In this section, we give more analysis on the real-world deployment of StereoWalker. Similar to other urban visual navigation models [39, 57, 58, 62], StereoWalker also requires a GPU for robot deployment, and it is not directly runnable on the Clearpath Jackal onboard CPU. We therefore employ a FastAPI-based interface to connect the robot with a remote GPU server for real-time inference, as we do not have NVIDIA Jetson hardware, which is used in previous works.

Despite this current limitation, the computational footprint of StereoWalker remains within the practical range of modern robotic platforms. Specifically, our model requires 2.89 GB of VRAM and 0.2 s per sample on an A100 GPU at inference time, compared to CityWalker which consumes 1.68 GB and 0.06 s per sample. This overhead remains manageable in our setting, as the model predicts five future waypoints spanning a five-second horizon. This allows the system to operate at a one-second inference interval, ensuring that new waypoint commands can be generated and executed between consecutive positions without causing stalls or instability in robot motion. As a result, even when accounting for network latency introduced by the FastAPI server, StereoWalker remains capable of real-robot deployment and achieves the best performance with minimal computation overhead compared to CityWalker, as evident in Fig. 4.